International Symposium
On Turbulence and Shear Flow
Phenomena (TSFP-9)
June 30 - July 3, 2015 *Melbourne, Australia*

LARGE EDDY SIMULATION OF A SIMPLIFIED LEAN PREMIXED GAS TURBINE COMBUSTOR

Christer Fureby
Defence Security Systems Technology
The Swedish Defence Research Agency (FOI)
SE 147 25 Tumba, Stockholm, Sweden
fureby@foi.se

Niklas Zettervall
Defence Security Systems Technology
The Swedish Defence Research Agency (FOI)
SE 147 25 Tumba, Stockholm, Sweden
niklas.zettervall@foi.se

Sayop Kim and **Suresh Menon**
School of Aerospace Engineering
Georgia Institute of Technology,
Atlanta, GA, 30332, USA
suresh.menon@ae.gatech.edu

ABSTRACT

Large-Eddy Simulation of swirl stabilized premixed flame in a gas turbine combustion is conducted using two different production codes using identical grid and chemical kinetics. The only differences then are in the types of subgrid closure for reaction-diffusion-turbulence coupling at the small scales. Results are reported for a range of reaction mechanisms from global two-step mechanisms to more complex 19-step and 25-step mechanisms.

INTRODUCTION

Large-Eddy Simulations (LES) of turbulent combustion in gas turbine type dump combustors have now become almost a standard practice both in academia and industry. The modeling strategy varies between the research groups, and sometimes it is very difficult to assess sensitivity of predictions to some of the underlying assumptions within the modeling tools. From a numerical point of view both structured and unstructured solvers have been employed (Granet *et al.,* 2013) with equally measurable successes (and sometimes) failures. Many studies employ flamelet assumptions (Hawkes & Cant, 2000; Mahesh *et al*., 2006) that are questionable when dealing with problems associated with lean blowout, ignition, etc., since the details of finite rate kinetics are not explicitly accounted for in the simulation. Studies in the past have also attempted to isolate the effect of numerics (scheme) from subgrid closures (Granet *et al*., 2013) but so far no assessment of the sensitivity of predictions to the complexity in finite-rate kinetics model (an open issue in itself) has been carried out. In this paper, we use a generic and simple swirl stabilized gas turbine combustor to investigate how subgrid closures that employ relatively detailed kinetics perform.

THE GELM6000 COMBUSTOR

The General Electric LM6000 is a turboshaft gas turbine engine with a power of ~41 kW. The GELM6000 is derived from the CF6-80C2 aircraft turbofan engine but includes variations designed to make it more suitable for marine propulsion, industrial power generation and marine power generation. The GELM600 engine has found wide use including power plants, fast ferries and high-speed ship applications. A simplified model of a single sector GELM-6000 combustor has been widely used by several research groups to test computational models for turbulent premixed combustion (Hura *et al*., 1998; Held & Mongia, 1998; Kim *et al*., 1999; Grinstein *et al*., 2002; Grinstein & Fureby, 2004; Granet *et al*., 2013). Experimental data of axial, tangential and radial velocities are available at the centerline and at two lines across the combustor at x/D=0.18 and 0.72, where D is the inlet diameter, at realistic conditions, p_0=6.0 atm and T_0=644 K, Kim *et al*. (1999).

This simplified combustor model, figure 1a, consists of a swirling air-fuel jet injected through a circular inlet, with a diameter of D=34 mm, in a rectangular, 70×102 mm^2, cross-sectional combustor equipped with a convergent extension and upper and lower, 3 mm wide, cooling air flow slits. The inlet conditions are given by the mean experimental axial, radial and tangential velocity profiles shown in figures 1b, with peak axial and tangential velocities reaching 120 m/s and 130 m/s, respectively. These analytical profiles are approximating the effects of the inlet-swirler arrangement, not provided by GEAE, Hura *et al*.,

1998; Held & Mongia, 1998). This lack of detailed geometrical information about the inlet-swirler arrangement unfortunately precludes any attempts at quantitative comparison between simulation results and experimental data, but facilitate code-to-code and model comparisons. Based on the mean inlet velocity and D, the Reynolds number is Re≈240,000, and the swirl number is S≈0.60. The fuel is methane and the equivalence ratio is ϕ=0.56. For this mixture the laminar flame speed and thickness are s_u≈0.31 m/s and δ_u≈0.09 mm, respectively. If the integral length scale and the rms velocity fluctuations are assumed to be ℓ_I=D and v′=30 m/s , respectively v′/s_u≈95 and ℓ_I/δ_u=340 , so that Ka≈50 and Da≈3.5, placing this combustor well into the thin reaction sheets regime.

To facilitate comparison with other simulation results, the same structured grid as used by Granet *et al*. (2013) is used, comprising 900 blocks, clustered around the swirler, flame, and at the combustor walls, and 1.9 million cells. A finer grid with 15.2 million cells is used to test grid independence. Dirichlet boundary conditions are used for all variables except for the pressure, p, at the inlet. At the outlet, all variables, except p, are extrapolated, whereas p is subject to a wave-transmissive boundary condition following Poinsot & Lele (1992). At the walls, a no-slip boundary condition is used together with zero Neumann conditions for all other variables. The simulations are initialized from a steady-state RANS simulation with a superimposed flame and combustion product region and are continued until the statistical moments has settled. The grid resolution in the combustor where the flame sits is between 0.2 and 0.6 mm, whereas further downstream the grid is coarsened to a resolution of about 3 mm. The laminar flame thickness, δ_u, is therefore between 2 and 6 times smaller than the grid resolution, necessitating the use of subgrid turbulence interaction models. In this study we employ different global and skeletal reaction mechanisms within subgrid closures to examine the influence of the reaction mechanism in LES studies.

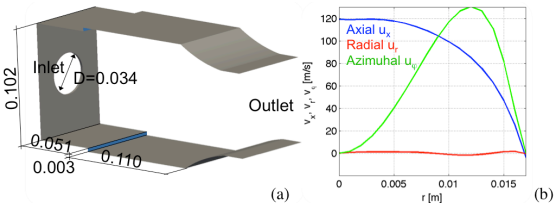

Figure 1. (a) Schematic of the GELM6000 combustor and (b) analytical axial, v_x, radial, v_r, and azimuthal, v_θ, velocity profiles at the combustor inlet.

LES COMBUSTION MODELING

The governing equations of turbulent combustion consist of the balance equations of mass, species concentrations momentum and energy, e.g. Menon & Fureby (2010). Due to the tremendous range of scales involved, ranging from the molecular scales of the chemical reactions to the scales of the geometry of the combustor, these equations must be simplified or low-pass filtered in order to be useful in applied simulations of turbulent combustion. This low-pass filtering introduces supplementary subgrid stress and flux terms, representing the effects of the smaller unresolved scales on the larger resolved scales, e.g. Sagaut (2001), that have to be modeled. In addition, the low-pass filtered reaction rates associated with the combustion chemistry needs also to be modeled, see Echekki (2009), to provide a closed set of equations. The modeling of the low-pass filtered reaction rates constitutes a major challenge due to the effects of the reaction mechanism and the non-linearity of the reaction rates. Here, we use two well-known LES combustion codes, using different numerical schemes and subgrid models, to examine both the effect of the reaction mechanisms and the closure modeling of the low-pass filtered reaction rates.

Reaction Mechanisms

In this study, five reaction mechanisms of increasing complexity are used to examine the influence of the reaction mechanism on the predicted flow and flame dynamics. These mechanisms are in order of increasing size: the 1- and 2-step global reaction mechanisms of Westbrook & Dryer (1981), WD1 and WD2; the 4-step global reaction mechanism of Jones & Lindstedt (1988), JL4; the 19-step skeletal reaction mechanism of Lu & Law (1988), LL19; the 20-step skeletal reaction mechanism of Sher & Refael (1988), SR20; and the 25-step skeletal reaction mechanism of Smooke & Giovangigli (1991), SG25. The JL4 reaction mechanism is, following Bulat *et al*. (2015), adjusted to better handle the influence of pressure, p, on the laminar flame speed, s_u, by modifying the pre-exponential factors such that $A_k=A_k^{p_0}(p/p_0)^{-0.865}$, with p_0=1.013 atm. Figure 2 compares these mechanisms with the reference GRI-3.0 mechanism, Frenklach *et al*., for laminar flames at 1 atm and 300 K, and at varying pressures.

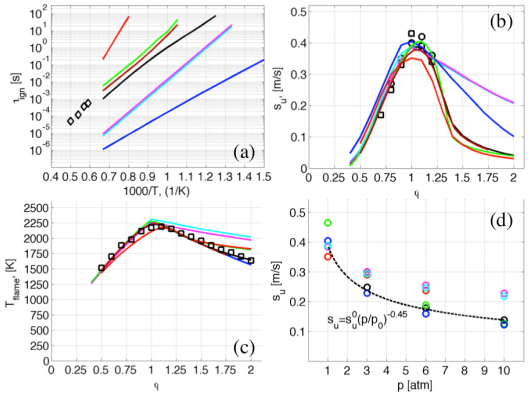

Figure 2. Comparison of (a) ignition delay times, τ_{ign}, (b) inar flame speeds, s_u, and (c) flame temperature, T_{flame}, at p=1 atm and (d) variation of s_u with pressure, p. Legend: (—) WD1, (—) WD2, (—) JL4, (—) LL19, (—) SR20, (—) SG25, (—) GRI-3.0 and (○, □) experimental data from Egolfopoulos *et al.* (1991 and 1994).

From figure 2a, comparing ignition delay times, τ_{ign}, we find a large spread between mechanism predictions with JL4 and SR20 showing the largest deviations from the GRI-3.0 mechanism, and SG25 and LL19 the best overall agreement. The laminar flame speed, s_u, in figure

2b, shows that the experimental data of Egolfopoulos *et al*. (1991 and 1994) agrees well with the reference GRI-3.0 mechanism predictions, and that the global WD1, WD2 and JL4 mechanisms all fail to predict the decay of s_u for rich flames. This is due to the absence of intermediate species, including several C-based species, also resulting in overprediction of the adiabatic flame temperature. However, the flame speed feature is captured well by the skeletal mechanisms LL19, SG25 and SR20. For lean situations, all mechanisms work reasonably well. The adiabatic flame temperature in figure 2c generally reveal good agreement between global, skeletal and detailed mechanisms and experimental data on the lean side, whereas significant differences occur on the rich side. This is consistent with the s_u predictions and is due to the absence of intermediate species, in particular the C-based species. LL19 and SG25 show the best overall agreement with the GRI-3.0 mechanism and the experimental data. The pressure variation in figure 2d reveals that only the skeletal mechanisms can capture the complex variation of s_u with pressure, p, being critical for successful gas turbine combustion modeling.

Codes Employed in this Study

In this study two different codes are used for modeling turbulent combustion in the GELM6000 combustor:

LESLIE is a structured multi-block multi-species finite volume compressible LES solver, developed by Georgia Institute of Technology. It uses various subgrid closure models and filtered reaction rate models. LESLIE is second order accurate in both space and time. The spatial scheme uses a hybrid MacCormack-MUSCL algorithm, where the MUSCL algorithm is employed only in regions of very high gradients.

Koodles is an unstructured multi-species finite volume compressible LES solver developed by FOI based on OpenFOAM, Weller *et al.* (1997) using a wide variety of subgrid models and filtered reaction rate models. Koodles is based on a compressible PISO-type algorithm together with a selection of time-integration and flux reconstruction algorithms. Here, a Crank-Nicholson time integration scheme is used together with linear flux reconstruction of the convective and diffusive terms. Koodles is second order accurate both in space and time. The combustion chemistry is integrated using a Strang-type operator-splitting scheme based on a Rosenbrock time-integration algorithm for stiff ODESs following Hairer & Wanner (1991).

Subgrid Flow Models

In order to close the low-pass filtered LES equations models for the subgrid stress and flux terms must be provided (Sagaut, 2001). Most combustion LES models are routinely based on an expanded Boussinesq approximation, the physical background of which is related to the well-known cascade process of turbulence (Sreenivasan & Stolovitzky, 1995). A consistent formulation was recently proposed by Li *et al*. (2009) making use of matrix exponentials, and here a first order approximation of this model is employed in which the subgrid time-scale τ_k is modeled as $\tau_k \approx k^{1/2}/\Delta$ in which the subgrid kinetic energy, k, satisfies a modeled transport equation following Schumann (1975) and Yoshizawa & Horiuti (1985). All simulations in this study are run using the same subgrid model with dynamically adjusted coefficients, Kim & Menon (1999).

Models for the Filtered Reaction Rates

Modeling the low-pass filtered reaction rates is extremely challenging since the chemical reactions typically occur at or even below the subgrid level. Numerous modeling approaches has been suggested including flamelet LES models, e.g. Pitsch (2005) and Hawkes & Cant (2000), thickened flame LES models, e.g. Colin *et al*., (2000), probability density function LES models (e.g. Jones *et al*., 2015 and Kim & Pope, 2014) partially stirred reactor LES models, Sabelnikov & Fureby, (2013) and linear eddy LES models, e.g. Menon & Patel, (2006). Here we have chosen to compare predictions from thickened flame, partially stirred reactor and linear eddy LES models.

LES Thickened Flame Model (LES-TFM): In the LES-TFM, e.g., Colin *et al*., (2000), the reaction rates are divided by a factor F, corresponding to the ratio between the grid resolution, Δ, and the laminar flame thickness, δ_u, and multiplied by a factor E corresponding to the ratio between the true and resolved flame wrinkling, Ξ. To maintain the laminar flame speed the species diffusivities the multiplied with the product of F and E.

LES Partially Stirred Reactor Model (LES-PaSR): The LES-PaSR model, Sabelnikov & Fureby, (2013), is a heterogeneous multi-scale model in which the filtered reaction rates are approximated as the product of the reacting volume fraction, γ^*, and the Arrhenius rates evaluated at the conditions, $\{Y_i^*, T^*\}$, of the reacting fine structures. The conditions of the reacting fine structures are obtained from local balance equations involving also the LES fields $\{\tilde{Y}_i, \tilde{T}\}$ whereas γ^* is modeled using the chemical time scale, $\tau_c=\delta_u/s_u$, and the subgrid time scale, τ_K.

LES Linear Eddy Model (LEMLES): In this model, the reaction-diffusion processes occurring within the small-scales are simulated inside each LES cell and coupled to the large-scale transport using a Lagrangian advection approach (Menon & Kerstein, 2011). Within the subgrid, the resolution is close to the Kolmogorov scale (typically 12-18 LEM cells are used in each LES cell) and thus the reaction kinetics are solved without any closure. The scalar field therefore, evolves by large-scale advection in 3D and a subgrid 1D LEM mixing process and the filtered species are predicted from the combined LEMLES approach. More details are in the cited references and therefore, not repeated.

RESULTS

Table 1 outlines the eleven LES computations performed in this study. As note above, all simulations employ the same grid using identical boundary conditions and subgrid flow models to facilitate comparison.

Tabel 1. Summary of simulations.

Run	*Comb. model*	*Subgrid model*	*Reaction mech.*	*Code*
1	LES-PaSR	OEEVM	WD2	Koodles
2			JL4	
3			SR20	
4			SG25	

5	LES-TFM	OEEVM	WD2	Koodles
6			JL4	
7			SR20	
8			SG25	
9	LESLEM	OEEVM	WD2	LESLIE
10			JL4	
11			LL19	

Figure 2 shows instantaneous combined temperature, fuel mass-fraction and vorticity renderings to illustrate the flow features in the GELM600 combustor from the LES-PaSR model using the SG25 mechanism. The temperature visualizations consist of volumetric renderings of T, from translucent blue, through gradually more opaque yellow, orange to red, whereas a gray iso-surface of Y_{CH4} at 75% of its inflow value is used to mark the flame. The vorticity visualization consists of iso-surfaces of the second invariant, λ_2, of the velocity gradient, $\nabla\tilde{\mathbf{v}}$, colored by the velocity magnitude from light gray, via green, to black.

The swirling inflow expands rapidly forming a recirculation zone in the center of the combustor and a toroidal-shaped recirculation zone between the dump plane and swirling inflow. The swirl creates a recirculation bubble and the flame is located between the central recirculation zone and the outer, toroidal-shaped, recirculation zone the combustor walls and the flame. The flame takes the shape of a short, wrenched expanding tube that fold back on itself when interacting with the head end of the central recirculation zone. The flame is stabilized and affected by the combined effect of swirl and reduction in axial velocity imposed by the central recirculation zone as the streamlines expand radially. In addition, high pressure and velocity gradient fluctuations are observed in the annual shear layer enclosing the swirling inflow. The effects of the upper and lower cooling air-flows can clearly be observed in the T visualizations.

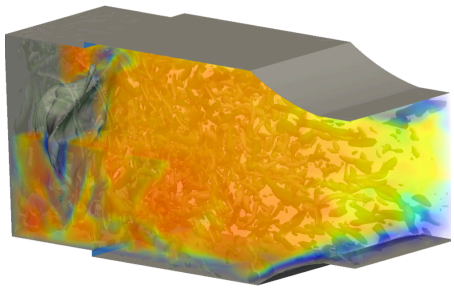

Figure 3. Volumetric renderings of the temperature combined with an iso-surface of the fuel mass fraction and iso-surfaces of the second invariant of the velocity gradient tensor, λ_2, colored by the velocity magnitude.

The overall behavior is generally similar for all combinations of codes, subgrid models, reaction mechanisms, and models for the filtered reaction rates, although with some differences, primarily attributed to the choice of reaction mechanism. Assessing similar results from all simulations suggests that: (i) The flow and vorticity is virtually unaffected by the choice of subgrid and filtered reaction rate models and by the choice of the reaction mechanism; (ii) The WD2 mechanism predicts a higher and more irregular T distribution than the other mechanisms; (iii) The SR39 mechanism results in a slightly lower and more unsteady combustor temperature as may be understood from figure 2; (iv) The LES-PaSR and TFM models act similarly, provided that the thickening factor, F, is slightly lower (1 to 3) than its proper value of between 5 and 10; (v) The LESLEM and LES-PaSR models behave very similar; (vi) The combination of LESLEM and the LL15 mechanism results in a slightly longer flame tube than the other model and mechanism combinations; (vii) Very similar results are found (with the LES-PaSR model and the SG25 mechanism) on a finer 15.0 million cell grid. The fact that more flow and flame scales are adequately resolved does not affect the flow or the flame, neither their statistics.

Figure 4 shows a few examples of different temperature and axial velocity distributions across the combustor. As mentioned, the velocity distribution is rather insensitive to the code, the model of the filtered reaction rates and the reaction mechanism, whereas the temperature is not. The velocity distributions also reveal a vortex breakdown bubble, in which the flow is recirculated due to the swirl caused by the adverse pressure gradient, located between x/D≈1 and 4. The WD2 mechanism overpredicts the peak temperature, which is also rather irregular, resulting in a temperature in excess of the flame temperature. The SR20, SG25 and LL19 mechanisms all predict the correct flame temperature but also result in smoother temperature fields. The Koodles predictions are found to give somewhat stronger shear layer shedding compared to the LESLIE predictions, which may be a result of the use of the hybrid MacCormack MUSCL algorithm in LESLIE.

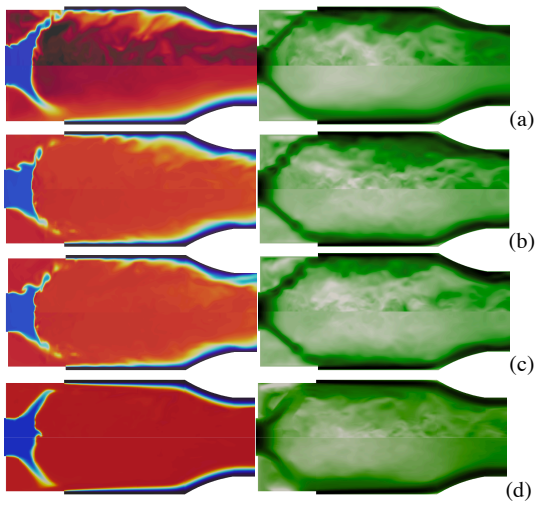

Figure 4. Instantaneous (upper panel) and time-averaged (lower panel) temperature (left) and velocity (right) contours for different models and reaction mechanisms: (a) LES-PaSR and WD2, (b) LES-PaSR and SG25, (c) LES-TFM and SG25 and (d) LESLEM with LL19.

Figure 5 shows profiles of the time-averaged axial velocity, $\langle\tilde{v}_x\rangle$, from the runs in Table 1 athwart the combustor at x/D=0.18, 0.72 and 2.33. Experimental data is avail-

able at x/D=0.18 and 0.72 but as the swirler arrangement is not present in the simulations considerable discrepancies between measured and predicted velocity profiles can be expected. This is particularly evident for $\langle \tilde{v}_x \rangle$ at both x/D=0.18, at which $\langle \tilde{v}_x \rangle$ is slightly underpredicted, and at x/D=0.72, at which is $\langle \tilde{v}_x \rangle$ is significantly underpredicted. All LES models, using the same inflow data, cf. figure 1b, however, show similar results, supporting the conjecture that the deviations are due to the lack of the swirler arrangements in the simulation models, and revealing that the quantitative difference between the predictions from the different code, model and mechanism combinations are rather small. The main differences occur at x/D=0.72 and appear to be primarily related to how LESLIE and Koodles capture the swirling and expanding shear layer from the inflow, which is more prominent in the Koodles predictions than in the LESLIE predictions.

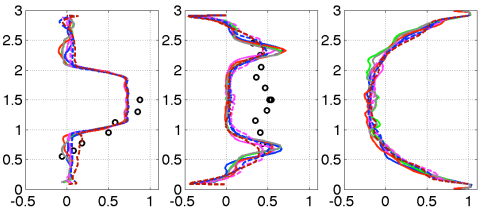

Figure 5. Profiles at x/D=0.18, 0.72 and 2.33, respectively, across the combustor of the time-averaged axial velocity, $\langle \tilde{v}_x \rangle$. Legend: (○) Experimental data, (—) PaSR+WD2, (—) PaSR+JL4, (—) PaSR+SG25, (—) PaSR+SR20, (—) TFM+SG25, (- -) LEM+WD2, (- -) LEM+JL4 and (- -) LEM +LL19.

Figure 6a and 6b shows profiles of the time-averaged tangential, $\langle \tilde{v}_t \rangle$, and radial, $\langle \tilde{v}_r \rangle$, velocity components, from the LES in Table 1 over the combustor at x/D=0.18, 0.72 and 2.33. These velocity distributions support the previous conjecture that the velocity distribution is virtually unaffected by the reaction mechanism, and show good agreement with the experimental data. $\langle \tilde{v}_t \rangle$ and $\langle \tilde{v}_r \rangle$ are not as influenced by the lack of the swirler arrangement in the simulations as compared to $\langle \tilde{v}_x \rangle$. The tangential and radial velocity distributions also reveal how fast the tangential velocity component decays with increasing distance from the burner mouth, and how small the radial velocity component is in comparison to the axial and tangential velocity components, and that $\tilde{v}_r$ increases along the swirling jet discharging from the burner mouth. As for the axial velocity Koodles predicts sharper tangential and radial velocity profiles than LESLIE, which is probably due to the slightly different flux reconstruction schemes used.

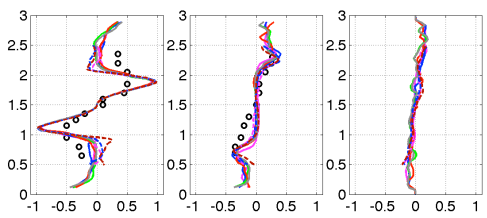

(a)

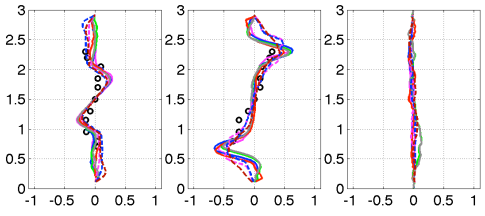

(b)

Figure 6. Profiles at x/D=0.18, 0.72 and 2.33, respectively, across the combustor of the time-averaged tangential, $\langle \tilde{v}_t \rangle$, and radial, $\langle \tilde{v}_r \rangle$, velocity components. For legend we refer to figure 5.

Figure 8 shows profiles of the time-averaged temperature, $\langle \tilde{T} \rangle$, from the runs in Table 1 athwart the combustor at x/D=0.18, 0.72 and 2.33. These profiles suggest, as seen in figure 4, that the WD2 mechanism results in a higher flame temperature than the other mechanisms, in fact with the temperature in excess of the adiabatic flame temperature, denoted by the dashed black line. The SR20 mechanism on the other hand results in a slightly lower temperature, just below the adiabatic flame temperature. This is particularly evident at x/D=0.72, a location which corresponds with the end of the wrenched flame tube and the beginning of the central recirculation region. Here we find that SR20 shows a slightly lower temperature, with a dip in the middle corresponding to a short flame tongue protruding from the main flame. It is also evident that the LEMLES predictions from the JL4 and LL19 mechanisms both show somewhat longer flame tube compared to the WD2 mechanism and compared to the predictions based on the LES-PaSR and TFM models, cf. figure 4.

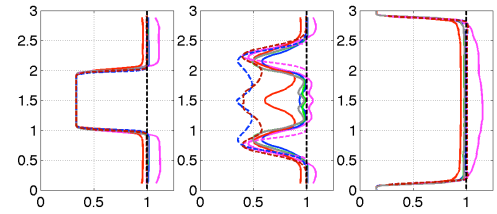

Figure 7. Profiles at x/D=0.18, 0.72 and 2.33, respectively, across the combustor of the time-averaged temperature, $\langle \tilde{T} \rangle$. For legend we refer to figure 5.

CONCLUDING REMARKS

The present study focused on evaluating the sensitivity of predictions to the use of finite-rate kinetics in a swirl stabilized combustion system. Two codes with different types of numerical architecture were used with identical grids, reaction kinetics and subgrid closure for the momentum transport. Closures for reaction diffusion differed in their complexity but for this particular case overall agreement was reasonable for all cases.

REFERENCES

Bulat G., Fedina E., Fureby C., Meier W. & Stopper U.; 2015 “Reacting Flow in a Industrial Gas Turbine Combustor: LES and Experimental Analysis”, *Proc. Comb. Inst.*, **35**, p. 3175.

Colin O., Ducros F., Veynante D. & Poinsot T.; 2000, "A Thickened Flame Model For Large Eddy Simulations of Turbulent Premixed Combustion", *Phys. Fluid*s, **12**, p 1843.

Echekki T.; 2009, "Topical review: Multiscale Methods in Turbulent Combustion: Strategies and Computational Challenges", *Comp. Sci. & Disc.* **2**, 013001.

Egolopoulos F. & Law C.; 1991, "An Experimental and Computational Study of the Burning Rates of Ultra-Lean to Moderately-Rich $H_2/O_2/N_2$ Laminar Flames with Pressure Variations", *Proc. Comb. Inst.*, **23**, p 333.

Frenklach F., Wang H., Yu C.L., Goldenberg M., Bowman C.T., Hanson R.K., Davidson D.F., Chang E.J., Smith G.P., Golden D.M., Gardiner W.C. & Lissianski V.; http://www.me.berkeley.edu/gri_mech.

Granet V., Menon S., Vermore O., Staffelbach G. & Poinsot T.; 2013, "Large Eddy Simulation of a Swirled Lean Premixed Gas Turbine Combustor: A Comparison of Two Compressible Codes", AIAA 2013-0171.

Grinstein F.F., Young T.R., Gutmark E.J., Li G., Hsiao G. & Mongia H.C.; 2002, "Flow Dynamics in a Swirl Combustor", *J. Turb.*, **3**, p 1468.

Grinstein F.F. & Fureby C.; 2004, "LES Studies of the Flow in a Swirl Gas Combustor", *Proc. Comb. Inst.*, **30**, p 1791.

Hairer E. & Wanner G.; 1991, "Solving Ordinary Differential Equations", II: Stiff and Differential-Algebraic Problems, 2nd Ed., Springer Verlag.

Hawkes E.R. & Cant R.S.; 2000, "A Flame Surface Density Approach to Large Eddy Simulation of Premixed Turbulent Combustion", *Proc. Comb. Inst.* **28**, p 51.

Hura H.S., Joshi N.D., Mongia H.C. & Tonouchi J., 1998, "Dry Low Emission Premixer CCD Modeling and Validation", ASME-98-GT-444.

Held T.J. & Mongia H.C.; 1998, "Application of a Partially Premixed Laminar Flamelet Model to a Low-Emission Gas Turbine Combustor", ASME-98-GT-217.

Jones W.P. & Lindstedt R.P.; 1988, "Global Reaction Schemes for Hydrocarbon Combustion, *Comb. Flame*, **73**, p 222.

Jones W.P., Marquis A.J. & Wang F.; 2015, "Large Eddy Simulation of a Premixed Propane Turbulent Bluff Body Flame using the Eulerian Stochastic Field Method", *Fuel*, **140**, p 514.

Kim J. Pope S.S.; 2014, "Effects of Combined Dimension Reduction and Tabulation on the Simulations of a Turbulent Premixed Flame using a Large-Eddy Simulation/Probability Density Function Method", *Comb. Theory & Modeling*, **18**, p388.

Kim W.-W., Menon S. & Mongia H.C.; 1999, "Large-Eddy Simulation of a Gas Turbine Combustor Flow", *Comb. Sci. & Tech.*, **143**, p 25.

Kim W.-W. & Menon S.; 1999, "A New Incompressible Solver for Large-Eddy Simulations", *Int. J. Num. Fluid Mech.*, **31**, p 983.

Li Y., Chevillard L., Eyink G. & Meneveau C.; 2009, "Matrix Exponential-based Closures for the Turbulent Subgrid-Scale Stress Tensor", *Phys. Rev. E.*, **79**, 016305.

Lu T. & Law C.K; 2008, "A Criterion based on Computational Singular Perturbation for the Identification of Quasi-Steady State Species: A Reduced Mechanism for Methane Oxidation with NO Chemistry", *Comb. Flame*, **154**, p 761.

Mahesh K., Constantinescu C., Apte S., Iaccarino G., Ham F. & Moin P.; 2006, "Large-Eddy Simulation of Reacting Turbulent Flows in Complex Geometries", *ASME J. Appl. Mech.*, **73**, p 375.

Menon S. & Fureby C.; 2010, "Computational Combustion", In En*cyclopedia of Aerospace Engineering*, Eds. Blockley R. & Shyy W., John Wiley & Sons.

Menon S. & Kerstein A.R.; 2011, "The Linear Eddy Model (LEM)" in Turbulent Combustion Modeling (T. Echekki and E. Mastorakos, Eds), *Fluid Dynamics and its Applications*, **95**, Springer, p 203.

Menon S. & Patel N.; 2006, "Subgrid Modeling for Simulation of Spray Combustion in Large-Scale Combustors", *AIAA J.*, **44**, p 709.

Pitsch H.; 2005, "A Consistent Level Set Formulation for Large-Eddy Simulation of Premixed Turbulent Combustion," *Comb. Flame*, **143**, p. 585.

Poinsot T.J. & Lele S.K.; 1992, "Boundary Conditions for Direct Simulation of Compressible Viscous Reacting Flows", *J. Comp. Phys.*, **101**, p 104.

Sabelnikov V. & Fureby C.; 2013, "LES Combustion Modeling for High Re Flames using a Multi-Phase Analogy", *Comb. Flame*, **160**, p 83.

Sagaut P.; 2001, "Large Eddy Simulation for Incompressible Flows", Springer Verlag, Heidelberg.

Sher E. & Refael S.; 1988, "A Simplified Reaction Scheme for the Combustion of Hydrogen Enriched Methane/Air Flames", *Comb. Sci. Tech.*, **59**, p 371.

Schumann U.; 1975, "Subgrid Scale Model for Finite Difference Simulations of Turbulent Flows in Plane Channels and Annuli", *J. Comp. Phys.*, **18**, p 376.

Smooke M.D. & Giovangigli V.; 1991, "Formulation of the Premixed and Nonpremixed Test Problems", In *Reduced Chemical Mechanisms and Asymptotic Approximations for Methane-Air Flames*, Smooke M.D., Ed., Springer-Verlag, New York, **384**, p 1.

Sreenivasan K.R. & Stolovitzky G.; 1995, "Turbulent Cascades", *J. Stat. Phys.*, **78**, p 311.

Vagelopoulos C., Egolfopoulos E. & Law C.; 1994, "Further Considerations on the Determination of Laminar Flame Speeds with the Counterflow Twin Flame Technique", *Proc. Comb. Inst.*, **25**, p 1341.

Weller H.G., Tabor G., Jasak H. & Fureby C.; 1997, "A Tensorial Approach to CFD using Object Oriented Techniques", *Comp. in Physics*, **12**, p 629.

Westbrook C.K. & Dryer F.L.; 1981, "Simplified Reaction Mechanisms for the Oxidation of Hydrocarbon Fuels in Flames", *Comb. Sci. Tech.*, **27**, p 31.

Yoshizawa A. & Horiuti K.; 1985, "A Statistically-Derived Subgrid Scale Kinetic Energy Model for Large Eddy Simulation of Turbulent Flows", *J. Phys. Soc. Japan*, **54**, p 283.